Open access • Posted Content • DOI:10.1101/2021.01.28.428430

Regulation of blood-brain barrier integrity and cognition by the microbiome-associated methylamines trimethylamine N-oxide and trimethylamine

Lesley Hoyles, Matthew G. Pontifex, Ildefonso Rodríguez-Ramiro, Ildefonso Rodríguez-Ramiro ...+13 more authors

Institutions: Nottingham Trent University, University of East Anglia, IMDEA, Queen Mary University of London ...+4 more institutions

Published on: 28 Jan 2021 - bioRxiv (Cold Spring Harbor Laboratory)

Topics: Trimethylamine N-oxide and Choline

Regulation of blood–brain barrier integrity and cognition by the microbiome-associated methylamines trimethylamine-*N*-oxide and trimethylamine

Lesley Hoyles[1]*, Matthew G. Pontifex[2], Ildefonso Rodriguez-Ramiro[2,3], M. Areeb Anis-Alavi[4], Tom Snelling[5], Egle Solito[6,7], Sonia Fonseca[8], Ana L. Carvalho[8], Simon R. Carding[2,8], Michael Müller[2], Robert C. Glen[5,9] David Vauzour[2] & Simon McArthur[4]*

[1]Department of Biosciences, School of Science and Technology, Nottingham Trent University, Clifton, Nottingham, UK
[2]Norwich Medical School, University of East Anglia, Norwich, UK
[3]Metabolic Syndrome Group, Madrid Institute for Advanced Studies (IMDEA) in Food, Madrid, E28049, Spain
[4]Institute of Dentistry, Barts & the London School of Medicine & Dentistry, Blizard Institute, Queen Mary University of London, London, UK
[5]Faculty of Medicine, Department of Metabolism, Digestion and Reproduction, Imperial College London, London, UK
[6]William Harvey Research Institute, Barts & the London School of Medicine & Dentistry, Queen Mary, University of London, London, UK
[7]Dipartimento di Medicina molecolare e Biotecnologie mediche, Federico II University, Naples, Italy
[8]The Gut Microbes and Health Research Programme, The Quadram Institute, Norwich Research Park, Norwich, UK
[9]Centre for Molecular Informatics, Department of Chemistry, University of Cambridge, Cambridge, UK

*__Corresponding authors:__ Lesley Hoyles, lesley.hoyles@ntu.ac.uk; Simon McArthur, s.mcarthur@qmul.ac.uk

Running title: Dietary methylamines affect the blood–brain barrier

Abbreviations: BBB, blood–brain barrier; DI, discrimination index; GO, gene ontology; KEGG, Kyoto Encyclopedia of Genes and Genomes; LPS, lipopolysaccharide; NOR, novel object recognition; SCFA, short-chain fatty acid; OFT, open field test; SPIA, signalling pathway impact analysis; TEER, transendothelial electrical resistance; TMA, trimethylamine; TMAO, trimethylamine *N*-oxide.

35

36 Supplementary materials associated with the article are available from figshare
37 (https://doi.org/10.6084/m9.figshare.13549334.v1).

ABSTRACT

Communication between the gut microbiota and the brain is primarily mediated *via* soluble microbe-derived metabolites, but the details of this pathway remain poorly defined. Methylamines produced by microbial metabolism of dietary choline and L-carnitine have received attention due to their proposed association with vascular disease, but their effects upon the cerebrovascular circulation have not hitherto been studied. Here we use an integrated *in vitro*/*in vivo* approach to show that physiologically relevant concentrations of the dietary methylamine trimethylamine *N*-oxide (TMAO) enhanced and protected blood-brain barrier (BBB) integrity, acting through the tight junction regulator annexin A1. In contrast, the TMAO precursor trimethylamine (TMA) impaired BBB function and disrupted tight junction integrity. Moreover, we show that long-term exposure to TMAO has beneficial effects upon cognition in mice, improving visual recognition memory. Our findings demonstrate a direct interaction of microbiome-associated metabolites with the mammalian BBB, with consequences for cerebrovascular and cognitive function.

INTRODUCTION

As the role of the gut microbiota in host physiology and disease is categorised, novel pathways through which these interactions are mediated continue to emerge. We and others recently identified the blood–brain barrier (BBB) as a target for gut microbe-derived short-chain fatty acid (SCFA) activity, with butyrate and propionate acting to promote BBB integrity and protect the cerebral vasculature from insult[1,2]. SCFAs represent just one of many classes of gut microbe-derived metabolites, with little known as to how these other classes may influence BBB function.

Dietary methylamines, such as choline, phosphatidylcholine, betaine and trimethylamine-*N*-oxide (TMAO), are a class of metabolites receiving considerable attention as modulators of vascular function[3,4], although the mechanism(s) by which they affect human physiology remain poorly understood. The aforementioned methylamines can be broken down by members of the gut microbiota into trimethylamine (TMA)[5], which is carried from the gut through the portal vasculature to the liver and rapidly converted into TMAO by flavin monooxygenases[6]. TMAO then enters the systemic circulation, reaching fasting plasma concentrations of between 2 and 40 μM in humans[7–9], prior to excretion through the urine[5]. Approximately ten-fold lower concentrations of TMA compared with TMAO are found in the circulation under normal physiological conditions.

Early observational work reported an apparent association between atherosclerosis and elevated levels of TMAO[10,11]. Similarly, pre-clinical studies demonstrate the damaging effects of supraphysiological TMAO doses in atherosclerosis-prone mice[12] and upon thrombus formation[13]. Despite this, the impact of TMAO upon the vasculature remains uncertain, with a number of detailed studies encompassing both human and murine systems failing to replicate these initial findings[14], instead suggesting that this negative relationship disappears upon correction for renal function[4,15–17]. This indicates that the raised TMAO levels may in fact reflect impaired excretion rather than being a causative factor of disease. Moreover, protective roles for TMAO have been reported in rodent models of hypertension[18], atherosclerosis[19] and non-alcoholic steatohepatitis[20] and we have previously shown TMAO to improve glucose homeostasis and insulin secretion in mice fed a high-fat diet[21]. Perhaps helping to clarify this apparent contradiction, recent studies have established that

intravenous treatment of rats with the TMAO precursor TMA, but not TMAO itself, increases mean arterial blood pressure[22]. Notably, the majority of reports describing associations of plasma TMAO with cardiovascular disease have not concurrently monitored levels of TMA; TMA but not TMAO has been shown to associate with severe aortic stenosis[22] and gestational diabetes risk[23].

Beyond vascular health, dietary methylamines have implications for cognition, with a positive correlation observed between choline intake and cognitive function in both humans[24,25] and mice[26,27]. In contrast, cerebrospinal fluid TMAO levels have been indicated as predictive of cognitive decline in Alzheimer's disease[28], while suppression of microbial TMA/TMAO production improves cognitive function in the murine APP/PS1 model of Alzheimer's disease[29]. Given the disparities in the literature regarding the effects of methylamines upon the vasculature, and our increasing awareness of the BBB as a major actor in the pathology of multiple neurological conditions, we investigated the effects of physiologically relevant concentrations of TMAO and its precursor TMA upon BBB integrity and cognitive behaviour.

METHODS

Endothelial cell culture

The human cerebromicrovascular endothelial cell line hCMEC/D3 was maintained and treated as described previously[2,30]. Cells bearing shRNA sequences targeting annexin A1 (*ANXA1*) or non-specific scramble sequences were produced as described previously[31]; the degree of *ANXA1* knock-down was confirmed by flow cytometry analysis (Suppl. Fig. 1). For all lines, cells were cultured to confluency in complete EBM-2MV microvascular endothelial cell growth medium (Promocell GmbH, Heidelberg, Germany), whereupon medium was replaced by EBM-2MV without VEGF and cells were further cultured for a minimum of 4 days to enable intercellular tight junction formation prior to experimentation.

In vitro barrier function assessments

Paracellular permeability and transendothelial electrical resistance (TEER) were measured on 100 % confluent hCMEC/D3 cultures polarised by growth on 24-well plate polyethylene terephthalate (PET) transwell inserts (surface area: 0.33 cm^2, pore size: 0.4 µm; Greiner Bio-One GmbH, Kremsmünster, Austria) coated with calf-skin collagen and fibronectin (Sigma-Aldrich, UK). The permeability of hCMEC/D3 cell monolayers to 70 kDa FITC-dextran (2 mg/ml) was measured as described previously[31–33]. TEER measurements were performed using a Millicell ERS-2 Voltohmmeter (Millipore, Watford, UK) and were expressed as $\Omega.cm^2$. In all cases, values obtained from cell-free inserts similarly coated with collagen and fibronectin were subtracted from the total values. In some cases, barrier integrity was tested by challenge with bacterial lipopolysaccharide (LPS). Confluent hCMEC/D3 monolayers were treated with TMAO or TMA for 12 h, whereupon LPS (*Escherichia coli* O111:B4; 50 ng/ml, comparable to circulating levels of LPS in human endotoxemia[34]) was added for a further 12 h, without wash-out. Barrier function characteristics were then interrogated as described above.

Cell adhesion assays

hCMEC/D3 cells were cultured to confluency on transwell inserts (0.4 µm pore size, 0.33 cm^2 diameter, Greiner Bio-One Gmbh, Austria) prior to 16 h treatment with 10 ng/ml TNFα. Monolayers were then incubated for 2 h with U937 monocytic cells pre-

labelled according to manufacturer's instructions with CMFDA cell tracker dye (ThermoFisher Scientific, UK). Co-cultures were washed vigorously with ice-cold PBS three times and fixed by incubation for 10 min in 1 % formaldehyde in 0.1 M PBS. Co-cultures were mounted and examined using an Axiovert 200M inverted microscope (Zeiss) equipped with a 20x objective lens. Images were captured with ZEN imaging software (Carl Zeiss Ltd, UK) and analysed using ImageJ 1.53c (National Institutes of Health, USA).

Microarrays

hCMEC/D3 cells were grown on 6-well plates coated with calf-skin collagen (Sigma-Aldrich, Gillingham, UK), and collected in TRIzol (Thermo-Fisher Scientific, UK) as described previously[2]. Total RNA was extracted using a TRIzol Plus RNA purification kit (Thermo-Fisher Scientific, UK) and quantified using a CLARIOstar spectrophotometer equipped with an LVis microplate (BMG Labtech GmbH, Germany).

Hybridization experiments were performed by Macrogen Inc. (Seoul, Republic of Korea) using Illumina HumanHT-12 v4.0 Expression BeadChips (Illumina Inc., San Diego, CA) as described previously[2].

Processing and analyses of array data

Raw data supplied by Macrogen were quality-checked, $\log_2$-transformed and loess-normalized (2 iterations) using affy[35]. Probe filtering and matching of probes not classified as 'Bad' or 'No match' to Entrez identifiers were done as described previously[2]. Average gene expression values were used for identification of differentially expressed genes. Array data have been deposited in ArrayExpress under accession number E-MTAB-6662. Normalized data are available (Supplementary Table 1).

Enrichr[36,37] was used to perform Gene Ontology (GO) analysis. Signaling Pathway Impact Analysis (SPIA) was used to determine whether Kyoto Encyclopedia of Genes and Genomes (KEGG) pathways were activated or inhibited in hCMEC/D3 cells exposed to TMAO or TMA[38]. Human KEGG pathways (KGML format) downloaded

from the KEGG PATHWAY database[39] were used for network (KEGGgraph, RBGL[40]) analysis.

Immunofluorescence microscopy

hCMEC/D3 cells were cultured on 24-well plate polyethylene terephthalate (PET) transwell inserts (surface area: 0.33 cm^2, pore size: 0.4 μm; Greiner Bio-One GmbH, Kremsmünster, Austria) coated with calf-skin collagen and fibronectin (Sigma-Aldrich, UK), prior to immunostaining according to standard protocols[2,31] and using a primary antibody directed against zonula occludens-1 (ZO-1; 1:100, ThermoFisher Scientific, UK) or Alexafluor 488-conjugated phalloidin (1:140, ThermoFisher Scientific, UK). Nuclei were counterstained with DAPI (Sigma-Aldrich, UK). Images were captured using an LSM880 confocal laser scanning microscope (Carl Zeiss Ltd, Cambridge, UK) fitted with 405 nm and 488 nm lasers, and a 63x oil immersion objective lens (NA, 1.4 mm, working distance, 0.17 mm). Images were captured with ZEN imaging software (Carl Zeiss Ltd, UK) and analysed using ImageJ 1.53c (National Institutes of Health, USA).

Flow cytometry analysis

Following experimental treatment, hCMEC/D3 cells were detached using 0.05% trypsin and incubated with an unconjugated rabbit polyclonal antibody directed against ANXA1 (1:1000, ThermoFisher Scientific, UK) on ice for 30 minutes, followed by incubation with an AF488-conjugated goat anti-rabbit secondary antibody (1:500, ThermoFisher Scientific, UK). Similarly detached hCMEC/D3 cells were incubated with APC-conjugated mouse monoclonal anti-BCRP (1:100, BD Biosciences, Oxford, UK), or PE-conjugated mouse monoclonal anti-MDR1A (1:100, BD Biosciences, UK) antibodies on ice for 30 minutes, alongside fluorescence minus one controls. Immunofluorescence was analysed for 20,000 events per treatment using a BD FACSCanto II (BD Biosciences, UK) flow cytometer; data were analysed using FlowJo 8.0 software (Treestar Inc., CA, USA).

Efflux transporter assays

Activity of the major efflux transporters P-glycoprotein and BCRP was determined through the use of commercially available assays (PREDEASY™ ATPase Assay Kits, Solvo Biotechnology Inc., Budapest, Hungary), performed according to the

manufacturer's instructions. Stepwise dose–response curves centred around reported physiological circulating concentrations of TMA (4.9 nM – 10.8 μM) and TMAO (0.5 μM – 1.08 mM) were constructed ($n = 4$) to investigate inhibitory effects of the methylamines upon transporter activity.

ELISA

Culture medium ANXA1 content was assayed by specific ELISA as described previously[41]. Serum TNFα and IL-1β concentrations were assayed using commercial ELISA kits according to the manufacturer's instructions (ThermoFisher Scientific, UK).

Animal experiments

All animal experiments were performed according to the UK Animals (Scientific Procedures) Act of 1986, under UK Home Office Project Licences PFA5C4F4F (short term studies) and 70/8710 (long term studies), following ethical review by the Animal Welfare and Ethical Review Boards of Queen Mary, University of London or the University of East Anglia, respectively. Wild-type male C57Bl/6J mice (Charles River Ltd., Harlow, UK) aged 8 weeks at the start of procedures were used throughout, with a group size of n=6 for short term studies and n=8 for long-term/behavioural analyses. Animals were housed in individually ventilated cages on a daily 12 h:12 h light/dark cycle with, unless otherwise indicated, *ad libitum* access to standard mouse chow and drinking water. Experimental procedures were started at 9 am to minimise variation associated with circadian rhythms.

Assessment of acute effects of TMAO on BBB integrity

Mice (n=4-6 per group) were injected i.p. with 1.8 mg/kg body weight TMAO in 100 μl saline vehicle, a dose calculated to approximate human circulating TMAO levels[42], followed 2 h, 6 h or 24 h later by assessment of Evans blue extravasation as described below. Alternatively, mice were injected i.p. with 3 mg/kg body weight LPS or 100 μl 0.9% saline vehicle, followed 2 h later by i.p. injection of either 1.8 mg/kg body weight TMAO or 100 μl 0.9% saline vehicle for assessment of Evans blue extravasation 2 h later. In both experiments, one hour before assessment animals were injected i.p. with 100 μl of a 2% (w/v) solution of Evans blue dye in 0.9 % saline (Sigma–Aldrich Ltd, Poole, UK). Dye was permitted to circulate for 1 h before animals were transcardially

perfused with 0.9% saline at 4 °C to remove circulating dye. Brains were removed, bisected and homogenized by maceration in 0.9% saline. Suspended macromolecules were precipitated by incubation with 60% trichloroacetic acid, and dye content of resulting supernatants was detected using a CLARIOstar spectrophotometer (BMG Labtech GmbH, Germany) alongside a standard curve of defined concentrations of Evans blue in the same buffer. Brain Evan's blue content was expressed as µg of dye per mg of brain tissue, normalized to circulating plasma concentrations.

Long-term LPS and TMAO treatments

To assess the long-term impact of both LPS and TMAO on cognitive performance, mice were divided into four groups (n=8 per group): 1) Water + PBS; 2) Water + TMAO; 3) LPS + PBS; 4) LPS + TMAO. C57Bl/6 mice were administered phosphate-buffered saline (PBS) or LPS (*Escherichia coli* O55:B5, Sigma-Aldrich, UK) via intraperitoneal (i.p.) injection (0.5 mg/kg/wk) for 8 weeks[43]. A final LPS treatment was administered the day before sacrifice for nine total injections. Body weights were recorded prior to each injection. TMAO was provided in the drinking water (500 mg/L) and water bottles replaced every other day. Drinking volumes were recorded before bottle change.

Processing and analyses of RNAseq data

Mice were transcardially perfused with 0.9% saline at 4 °C to remove circulating blood, and brains were removed and collected into RNAlater (Thermofisher Scientific Ltd., UK) prior to storage at -20 °C for later analysis. Whole brain total RNA was extracted using a PureLink RNA Mini Kit (Thermofisher Scientific Ltd., UK) and quantified using a CLARIOstar spectrophotometer equipped with an LVis microplate (BMG Labtech GmbH, Germany). RNA samples (*n*=3 TMAO, *n*=3 control) were sent to Macrogen Inc. (Republic of Korea) where they were subject to quality checks (RIN analysis); libraries were prepared (TruSeq Stranded mRNA LT Sample Prep Kit) for paired-end (2x 100 nt) sequencing on an Illumina HiSeq 4000 apparatus. Raw RNAseq sequence data (delivered in fastq format) were processed in house as follows. Reads were mapped onto the mouse genome (mm10) using HISAT2 v2.1.0[44]. Number of reads in each sample that mapped to genes in the BAM files returned by HISAT2 was determined using featureCounts v1.6.4[45]. Entrez gene identifiers were converted to gene symbols using *Mus musculus* annotations downloaded from NCBI on 26 November 2020; only those genes with valid Entrez gene identifiers were retained in analyses. Raw RNAseq

data have been deposited with ArrayExpress under accession number E-MTAB-9869. Significantly differentially expressed genes (P<0.1) were analysed by mouse KEGG pathway over-representation analysis using Enrichr and manual curation.

Behavioural analyses

Behavioural tests were performed in the order they are introduced below. Apparatus was cleaned using 70 % ethanol upon completion of each trial, eliminating any residual odour.

Open field test (OFT) was conducted as previously described[46]. Briefly, mice were placed in the centre of the OFT, a grey 50 x 50 x 50 cm apparatus illuminated with low lux (100 lux) lighting. Total travel distance and time spent in the centre of the field was determined at 5 min with a video tracking system (Smart 3.0 tracking software, Panlab, Kent, UK).

The novel object recognition (NOR), a measure of recognition memory, was performed as described previously[47,48], with slight modifications. Briefly, on day 1 mice were habituated in a grey 50 x 50 x 50 cm apparatus illuminated with low lux (100 lux) lighting, mice were placed into the empty maze and allowed to move freely for 10 min. On day 2, mice were conditioned to a single object for a 10 min period. On day 3, mice were placed into the same experimental area in the presence of two identical objects for 15 min, after which they were returned to their respective cages and an inter-trial interval of 1 h was observed. One familiar object was replaced with a novel object. Mice were placed back within the testing area for a final 10 min. Videos were analysed for a 5 min period, after which if an accumulative total of 15 s with both objects failed to be reached, analysis continued for the full 10 min or until 15 s was achieved. Those not achieving 15 s were excluded from the analysis[49]. A discrimination index (DI) was calculated as follows: DI = (TN−TF)/(TN+TF), where TN is the time spent exploring the novel object and TF is the time spent exploring the familiar object.

Y-maze spontaneous alternation test, a measure of spatial working memory, was performed on the final day of behavioural testing as previously described[50]. Briefly, the Y-maze apparatus comprised white Plexiglas (dimensions 38.5 × 8 × 13 cm, spaced 120° apart) and was illuminated with low lux (100 lux) lighting. Mice were placed in the

maze and allowed to explore freely for 7 min while tracking software recorded zone transitioning and locomotor activity (Smart 3.0 tracking software, Panlab, Kent, UK). Spontaneous alternation was calculated using the following formula: Spontaneous Alternation = (Number of alternations/ Total Arm entries - 2) x 100.

Extravasation assay and sample processing following long-term treatment

Twenty-four hours after the final injection of LPS, mice were injected i.p. with 200 µl of 2% sodium fluorescein in sterile ddH_2O and anesthetized 30 min later with isoflurane (1.5%) in a mixture of nitrous oxide (70%), and oxygen (30%). Once sedated, blood was collected by cardiac puncture and centrifuged at 1,500 × g for 15 min at 4 °C to collect the serum. The samples were analysed immediately for sodium fluorescein extravasation or snap-frozen in liquid nitrogen and stored at -80 °C until further analysis.

Mice were then transcardially perfused with saline containing 10 kU/ml heparin (Sigma, Devon, UK). Dissected left hemi-brains were fixed in 4% PFA for 24 h and embedded into paraffin before being processed for immunohistochemical analysis. Right hemi-brains were stored at -80 °C until further analysis; cerebellums were processed immediately for the sodium fluorescein extravasation assay. Cleared volume of sodium fluorescein that passed from the plasma into the brain was calculated as described previously[43].

Statistical analyses

Sample sizes were calculated to detect differences of 15 % or more with a power of 0.85 and α set at 5 %, calculations being informed by previously published data[2,31]. *In vitro* experimental data (except those for *in vitro* microarray experiments) are expressed as mean ± SEM, with a minimum of n = 3 independent experiments performed in triplicate for all studies. In all cases, normality of distribution was established using the Shapiro–Wilks test, followed by analysis with two-tailed Student's *t*-tests to compare two groups or, for multiple comparison analysis, 1- or 2-way ANOVA followed by Tukey's HSD *post hoc* test. Where data were not normally distributed, non-parametric analysis was performed using the Wilcoxon signed rank test. A P value of less than or equal to 5 % was considered significant. Differentially expressed genes were identified in microarray data using LIMMA (Ritchie *et al*, 2015);

342 *P* values were corrected for multiple testing using the Benjamini–Hochberg procedure
343 (False Discovery Rate); a *P* value of less than or equal to 10 % was considered
344 significant in this case; *n* = 5 for control, TMAO and TMA groups. Significantly
345 differentially expressed genes (P_{FDR}<0.1) in RNAseq data (Supplementary Table 11)
346 were identified using DESeq2 v1.22.1[51].
347

RESULTS

To provide an initial assessment of the effects of the methylamines TMA and TMAO upon the BBB we used a well-established *in vitro* BBB model, hCMEC/D3 immortalised human cerebromicrovascular cell monolayers grown under polarising conditions on a Transwell filter, examining two key barrier properties: paracellular permeability to a protein-sized tracer and TEER. Exposure of hCMEC/D3 cells for 24 h to TMA (0-40 μM) caused a clear dose-dependent increase in paracellular permeability to 70 kDa FITC-dextran (Fig. 1A), with normal circulating levels (0.4 μM) of TMA and upwards significantly enhancing permeability. In contrast, exposure for 24 h to TMAO (0-4000 μM) caused a biphasic dose-dependent response (Fig. 1A), with normal circulating concentrations (40 μM) significantly reducing permeability to the tracer, an effect lost at 10-fold greater TMAO concentrations and reversed at 100-fold greater TMAO (4 mM), where a significant increase in paracellular permeability was apparent. In contrast, TMA had no effect upon TEER at any concentration studied, while TMAO enhanced TEER by approximately 65%, an effect that was notably dose-independent (Fig. 1B).

The physical barrier that the BBB provides is only one aspect by which it separates the brain parenchymal environment from the periphery, equally important is the immunological barrier that it represents. To model this, we employed a simple system in which adhesion of CMFDA-labelled U937 monocytic cells to TNFα-activated (10 ng/ml, 16 h) hCMEC/D3 monolayers was quantified in response to TMA or TMAO treatment. Treatment with a physiologically relevant concentration of TMA (0.4 μM[42], 24 h post-TNFα) had no effect on the density of adherent U937 cells, but exposure of hCMEC/D3 monolayers to physiological levels of TMAO (40 μM[42], 24 h post-TNFα) significantly reduced U937 cell adhesion by approximately 50% compared to cultures stimulated with TNFα alone (Fig. 1C).

The endothelial cells of the BBB express numerous efflux transporter proteins that serve to limit entry of endogenous and exogenous molecules into the parenchyma, with BCRP and P-glycoprotein being two of the most important. Consequently, we examined whether treatment with TMA or TMAO affected function or expression of either of these two transporters. Using commercially available *in vitro* assays, neither

methylamine affected BCRP or P-glycoprotein activity across a wide concentration range (TMA: 4.9 nM to 10.8 µM; TMAO 0.5 µM to 1.08 mM) (Suppl. Fig. 2A-D). Similarly, treatment of hCMEC/D3 cells for 24 h with physiologically relevant concentrations of TMA (0.4 µM) or TMAO (40 µM) was without effect on cell surface expression of either BCRP or P-glycoprotein (Suppl. Fig. 2E-F).

Methylamine-induced changes in gene expression

Having identified significant TMA-/TMAO-induced functional changes in endothelial barrier characteristics *in vitro*, we undertook a microarray analysis of hCMEC/D3 cells treated with either TMA (0.4 µM, 24 h) or TMAO (40 µM, 24 h) to investigate the transcriptional changes underlying these effects. Treatment with TMA had a significant (P_{FDR}<0.1) effect on 49 genes, with the expression of 39 upregulated and 10 downregulated (Fig 2A, Supplementary Table 2). In contrast, treatment with TMAO had a significant (P_{FDR}<0.1) effect on 440 genes with 341 upregulated and 99 downregulated (Fig. 2B, Supplementary Table 3). *FMO3* gene expression was not affected by TMA or TMAO at the physiological concentrations employed (Suppl. Fig. 3).

SPIA of the 440 TMAO-affected genes showed activation of the tight junction pathway (P = 0.031), but significance was lost after correction for multiple testing (Supplementary Table 4). No pathways were shown to be activated or inactivated by the 49 TMA-affected genes (data not shown).

Gene ontology (GO) analysis was performed on TMA- and TMAO-regulated genes using Enrichr[36,37]. TMA up-regulated and down-regulated genes were significantly (P_{FDR}<0.2) associated with processes indicative of a degree of cellular stress (Fig 2C, Supplementary Table 5, Supplementary Table 6). In contrast, genes up-regulated by TMAO treatment were associated with regulation of the cytoskeleton and cell morphology and with actin bundle formation (P_{FDR}<0.2), whereas pathways associated with inflammatory signalling were down-regulated (Fig 2D, Supplementary Table 7, Supplementary Table 8).

We then assessed the topology of a directional network of the 440 TMAO-associated genes mapped onto all human KEGG pathways. In line with the GO analysis described

above, a number of genes of differing function were regulated by TMAO treatment, with two principal groupings being particularly evident, namely those associated with aspects of cellular metabolism and with regulation of actin cytoskeletal dynamics (Figure 2E). Finally, we compared the 19,309 genes represented on the microarray with a set of 203 genes[2] known to be associated with the BBB. While TMA treatment had no significant effects on expression of these genes (Supplementary Table 9), TMAO significantly (P_{FDR}<0.1) upregulated expression of four genes from this set associated with transporter proteins and barrier integrity (Table 1, Supplementary Table 10).

Given these transcriptional indications, and the fact that the restrictive properties of the BBB are largely governed by inter-endothelial cell tight junctions linked *via* the zonula occludens complex to the actin cytoskeleton[52], we hypothesised that TMA and TMAO may affect barrier permeability through modification of the links between tight junctions and the actin cytoskeleton. Confocal immunofluorescence microscopy of hCMEC/D3 monolayers treated with a physiologically relevant concentration of TMA (0.4 μM, 24 h) or TMAO (40 μM, 24 h) revealed clear changes to both ZO-1 and fibrillar actin disposition within cells (Fig. 2F). Compared to untreated cells in which both ZO-1 and F-actin fibres clearly defined the cellular perimeter, cells treated with TMA exhibited a broken, patchy distribution of perimeter ZO-1 expression, and the appearance of marked cytoplasmic F-actin stress fibres. In contrast, cells treated with TMAO showed little change in ZO-1 distribution, but a marked enhancement of cortical F-actin fibre thickness and intensity.

The actions of TMAO are mediated through annexin A1 signalling

Of the four BBB-associated genes identified as upregulated by TMAO, *ANXA1* is of particular interest as we have previously shown this protein to regulate BBB tightness *in vitro* and *in vivo* through modulation of the actin cytoskeleton[53]. Examination of ANXA1 expression in hCMEC/D3 cells revealed that while total cellular levels of the protein were not changed by either TMA (0.4 μM, 24 h) or TMAO (40 μM, 24 h) treatment (Fig. 3A), TMA significantly suppressed and TMAO significantly augmented medium ANXA1 content (Fig. 3B), a finding of interest given that autocrine/paracrine effects are a major route of ANXA1 action[54].

To establish the importance of ANXA1 in mediating the effects of TMAO, we investigated the effects of its depletion through use of hCMEC/D3 clones stably transfected with shRNA sequences targeting *ANXA1* mRNA (Suppl. Fig. 1). Suppression of *ANXA1* expression significantly inhibited the effects of TMAO (40 μM, 24 h) upon both paracellular permeability and TEER (Fig. 3C-D), an effect not seen in cells bearing non-targeting scramble shRNA sequences. The actions of ANXA1 are mediated to a large extent through the G protein-coupled receptor formyl peptide receptor 2 (FPR2)[55]. Hence, we investigated how inclusion of a well-characterised antagonist to this receptor, WRW_4 (10 μM, 10 min pre-treatment), would affect the functional response to TMAO. Pre-treatment with WRW_4 was able to significantly attenuate the effects of TMAO treatment on both TEER (Fig. 3E) and paracellular permeability (Fig. 3F), further indicating the role of ANXA1 signalling as the principal mediator of TMAO actions on hCMEC/D3 cells.

Acute beneficial effects of TMAO treatment in vivo

While hCMEC/D3 endothelial cells are a widely used and generally representative model, they cannot reflect all aspects of the multicellular neurovascular unit that underlies BBB function, hence we investigated whether the beneficial effects of TMAO identified *in vitro* translate to an *in vivo* situation. Initial studies revealed that systemic administration of TMAO to wild-type male mice (1.8 mg/kg, i.p.) induced a time-dependent reduction in BBB permeability to the tracer Evans blue (2 % in saline, 100 μl, i.p.), with a significant reduction in dye extravasation to the brain parenchyma being apparent 2 h following TMAO administration, an effect lost at longer time-points (Fig. 4A), presumably due to the relatively short plasma half-life of TMAO *in vivo*[56]. To further investigate this effect of TMAO, we employed a simple model of enhanced BBB permeability, namely acute peripheral administration of bacterial LPS[31]. Treatment with LPS (*E. coli* O111:B4, 3 mg/kg, i.p.) significantly enhanced intraparenchymal extravasation of Evans blue within 4 h, an effect significantly attenuated by subsequent treatment with TMAO (1.8 mg/kg, i.p.) 2 h post-LPS (Fig. 4B), further confirming a beneficial action of TMAO at physiological concentrations upon the BBB *in vivo*.

TMAO treatment rapidly alters brain transcriptional activity

To investigate the wider actions of TMAO upon the brain we performed whole brain RNAseq transcriptomic analysis of wild-type male mice 2 h following TMAO administration (1.8 mg/kg i.p.). We identified 76 significantly differentially expressed genes (P_{FDR}<0.1), with expression of 41 upregulated and 35 downregulated (Figure 5A; Supplementary Table 11). KEGG pathway analysis using Enrichr identified a number of significantly regulated murine pathways (Figure 5B), including oxidative phosphorylation, Parkinson's disease and Alzheimer's disease. Closer analysis of regulated genes identified a number of general groupings (Figure 5C), with downregulated genes associated with the mitochondrial respiratory chain (*COX1*, *COX3*, *ATP6*, *ND4L*, *CYTB*, *ND1*, *ND3*, *ND4*, *ND6*) and ribosomal function (*mt-Rnr2*, *mt-Rnr1*, *Rps23rg1*) and upregulated genes associated with cellular or axonal growth (*Nme7*, *B3gat2*, *Fuz*, *Nefm*, *Basp1*, *Mtg1*, *Vps37a*, *Smim1*, *Araf*). Of the 203 BBB-associated human genes previously identified[2], 197 had matches in our mouse brain data set. Here, two genes were identified as significantly differentially expressed at P_{FDR}<0.1: reduced *Cpe* (carboxypeptidase E) and increased *App* (amyloid precursor protein) expression (Figure 5D; Supplementary Table 12).

Chronic low-dose TMAO treatment prevents LPS-induced BBB disruption and memory impairment

The fundamental role of the BBB is to protect the brain, preserving its homeostatic environment; damage to BBB integrity is therefore detrimental, and is believed to directly contribute towards cognitive impairment[57–59]. Having shown TMAO to exert a protective effect upon BBB function/integrity in response to acute inflammatory insult, we next examined whether a similar effect held true for chronic conditions, and whether this protection extended to cognition. TMAO was administered to male C57Bl/6J mice through drinking water (0.5 mg/ml) over 2 months, in combination with chronic low-dose LPS administration (0.5 mg/kg/week, i.p.) to model a mild inflammatory stress known to impact cognitive behaviour[43]. There were no differences in volumes of water drunk or, where relevant, final consumption of TMAO between any groups (Table 2). The serum inflammatory cytokines TNFα and IL-1β were both nominally elevated in response to LPS treatment, although not reaching statistical significance, indicating a sub-clinical inflammatory response; TMAO had no effect on TNFα nor IL-1β levels (Suppl. Fig. 4). Notably, animals exposed to LPS exhibited a

515 significant reduction in body weight gain compared to their untreated counterparts, an
516 effect reversed by TMAO treatment (Fig. 6A). Treatment with LPS increased
517 cerebellar FITC extravasation, an effect that was prevented by TMAO treatment,
518 although this did not reach statistical significance on *post hoc* analysis (Fig. 6B). To
519 corroborate these findings, we investigated a second marker of impaired BBB integrity,
520 confocal microscopic detection of brain perivascular IgG deposition. In comparison
521 with sham-treated animals, exposure to LPS caused a significant accumulation of IgG
522 in the perivascular compartment, an effect prevented by TMAO treatment (Fig. 6C).
523
524 The OFT confirmed neither LPS nor TMAO treatment affected motor function, with
525 movement speed and distance travelled comparable across treatment groups (Fig.
526 6D-E). Similarly, no effect was apparent on the proportion of time animals spent in the
527 centre of the field, suggesting limited effects upon anxiety (Fig. 6F). Working memory,
528 however, determined via NOR indicated a significant reduction in performance in
529 animals exposed to LPS, a behavioural deficit notably prevented in animals co-treated
530 with TMAO (Fig. 6G). In contrast, no effect of either LPS or TMAO treatment was
531 apparent in the Y-maze spontaneous alternation task (Fig. 6H) or in distance travelled
532 during this task (Fig. 6I), indicating no differences in spatial memory.
533
534

DISCUSSION

The relationship between the BBB and cognitive behaviour is complex and far from being fully understood, but it is clear from both human and animal studies that deficits in barrier integrity can exert a profound and deleterious effect upon memory, language and executive function[60–63]. Indeed, BBB impairment is among the first events to occur in the course of Alzheimer's disease, and may aggravate the pathological processes that underlie the condition[64]. Strategies to promote BBB function may thus have significant value in helping to protect the brain from progressive neurological diseases such as dementia. In this study we identify novel and distinct roles for the microbiome-associated dietary methylamines TMA and TMAO in regulating BBB function *in vitro* and *in vivo* and provide evidence that the beneficial action of TMAO upon the BBB coincides with similar protective effects upon cognition. These data reinforce the position of the cerebral vasculature as a major target for the gut-brain axis, and extend our knowledge of its interactions with microbial metabolites beyond SCFAs[1,2] to another major class of molecules, the dietary methylamines.

Notably, our data show that while both TMA and TMAO have activity upon the endothelium, there is a marked distinction between their effects despite their close structural similarity. TMA, the direct product of microbial choline, L-carnitine and TMAO metabolism in the upper gut[5], had a deleterious effect upon the endothelium, disrupting cytoskeletal arrangement, inducing signs of metabolic stress and ultimately impairing endothelial barrier integrity. In contrast, TMAO, largely derived from hepatic FMO3-mediated oxidation of TMA taken up from the gut via the hepatic portal vein[6], was beneficial for cerebral vascular integrity *in vitro* and *in vivo*. These differences suggest that host conversion of TMA (a gas) to TMAO (a stable metabolite) may be an effective detoxification pathway, emphasising the importance of host metabolic pathways in modulating communication in the gut-brain axis, and underlining the importance of using a systems-level approach to understand the interactions between the host and its resident microbiota.

TMAO and cognitive function

Numerous groups have investigated the putative relationship between TMAO and cognition following reports of an association between cerebrospinal fluid TMAO

content and Alzheimer's disease[28], with negative correlations between plasma TMAO content and cognitive function having been identified in both clinical[65–67] and experimental[29,68,69] settings. Whether this relationship is truly deterministic remains unclear, however, as the role of the immediate precursor to TMAO, TMA, in cognition and vascular function has largely been overlooked. This omission may be important in light of studies reporting negative correlations between cognitive impairment and serum TMA[70–72] and our own data showing a potent detrimental effect of physiological levels of TMA upon the cerebrovascular endothelium *in vitro*. Given that TMA has been shown to be detrimental in contexts other than cognitive function[22,23], the contribution that this metabolite plays in disease is evidently in need of closer attention.

Interpreting associations between circulating TMAO and cognition is further complicated by studies indicating that consumption of the TMAO precursors choline and L-carnitine can improve cognitive function[24,25,73], evidence that patients with Parkinson's disease have lower circulating TMAO than healthy controls[74], and more recent Mendelian randomisation analysis indicating that serum TMAO and Alzheimer's disease are not causally related[75]. Given this background, our data indicating that physiologically relevant concentrations of TMAO have positive effects upon both BBB integrity and cognition *in vivo* thus serve as a useful counterweight to population-level correlation studies. Interestingly, a number of previous interventional studies have been performed in mice, suggesting that substantially higher doses of TMAO may have detrimental effects upon learning and memory[68,69,76], although as we and others[77] have identified dose-dependency in the effects of TMAO *in vitro*, it seems plausible that this may reflect a similar phenomenon *in vivo*. The importance of investigating the impact of TMAO under physiologically relevant conditions is further emphasised by a recent study showing TMAO treatment to impair novel object recognition in mice[65], ostensibly an opposite finding to our data achieved with a similar dosing regimen. Importantly, however, mice in this study were maintained on a reduced choline diet, a condition known to alter hepatic metabolism[78]; what impact such changes might have on handling of (TMA and) TMAO by the body is unknown. These discrepancies may be instructive in guarding against incautious extrapolation of TMAO effects from healthy to diseased populations.

Could TMAO contribute to the beneficial effects of a seafood-rich diet?

Consumption of a diet rich in fish and other seafood, known to provide significant quantities of TMAO[79], associates with a reduced risk of cognitive decline[80,81] and protection against cerebrovascular disease[82]. These effects have in large part been attributed to beneficial actions of the omega-3 polyunsaturated fatty acids[83], although there is little evidence that their direct supplementation improves cognitive function[84] or stroke risk[85]. Here we provide evidence that another component of a seafood-rich diet, TMAO, has protective effects on the cerebral vasculature and upon cognition, indicating that broadening the scope of nutritional analyses beyond the omega-3 fatty acids may be worthwhile. In particular, we demonstrate that TMAO acts to stimulate endothelial secretion of a major regulator of BBB permeability, ANXA1[53], leading *via* autocrine/paracrine activation of its receptor FPR2 to cytoskeletal actin rearrangement and enhanced BBB integrity.

This novel interaction between TMAO and ANXA1 may have implications beyond BBB integrity, given that ANXA1 is a major mediator of inflammatory resolution[86], and highlighted by our finding that TMAO treatment inhibited model immune cell adhesion to activated endothelia *in vitro*. As with the link between a seafood-rich diet and cerebrovascular health, fish consumption has been associated with reduced inflammatory disease, again attributed primarily to a role for omega-3 fatty acids[87]. While it is too early to definitively claim an anti-inflammatory role for dietary methylamines, particularly given the opposing actions of TMA and TMAO, our data do suggest that investigation of the bioactive properties of seafood-rich diets should progress beyond omega-3 fatty acids to focus on other potential contributors.

Conclusions

Interest in the role played by the gut microbiota in communication through the gut-brain axis has grown dramatically in the last few years, with much attention focused on the mediating actions of microbe-derived metabolites[88]. While a number of studies have shown patterns in microbial metabolite production that associate with different brain functions[89], detailed understanding of the role of individual molecules remains in its infancy, with defined roles characterised for only a subset of the many molecules known to be released by gut microbes. Here we show that the dietary methylamine TMAO can beneficially modulate both BBB integrity and cognitive function *in vivo*, providing direct mechanistic evidence for a positive role of this microbiome-associated

637 metabolite, and reinforce the position of the BBB as an interface in the gut-brain axis.
638 Notably, the positive effects of TMAO that we report stand in contrast to previous work
639 describing deleterious effects of TMAO exposure at high concentrations or under non-
640 physiological conditions[77], emphasising the importance of taking a holistic approach
641 to understanding gut microbiota-host interactions.
642
643

COMPETING INTERESTS

The authors declare that they have no competing interests.

ACKNOWLEDGEMENTS

This work was funded by Alzheimer's Research UK Pilot Grant No. ARUK-PPG2016B-6. PREDEASY™ efflux transporter analysis kits were generously provided through the SOLVO Biotechnology Research and Academic Collaborative Transporter Studies (ReACTS) Program. This work used the computing resources of the UK MEDical BIOinformatics partnership – aggregation, integration, visualisation and analysis of large, complex data (UK MED-BIO), which was supported by the Medical Research Council (grant number MR/L01632X/1). SF was supported by Fundación Alfonso Martín Escudero. TS was supported by a bursary from the Imperial College London Undergraduate Research Opportunities Programme. LH, DV and SM designed the experiments. SM performed cellular assays and acute *in vivo* analyses. TS carried out the initial permeability and TEER assays. MAA performed IgG extravasation studies. ES produced and provided shRNA treated hCMEC/D3 clones. LH undertook all processing and analyses of transcriptomic data. RCG provided valuable insight and advice throughout the project. DV, MP, IR and MM performed the chronic *in vivo* LPS challenge study and undertook all analyses of behavioural data. SRC, ALC and SF contributed to preliminary animal work. LH, DV and SM wrote the manuscript. All authors read and approved the final version of the manuscript.

REFERENCES

1. Braniste, V. *et al.* The gut microbiota influences blood-brain barrier permeability in mice. *Sci. Transl. Med.* **6**, 263ra158-263ra158 (2014).
2. Hoyles, L. *et al.* Microbiome–host systems interactions: protective effects of propionate upon the blood–brain barrier. *Microbiome 2018 61* **6**, 55–55 (2018).
3. Tang, W. H. W. & Hazen, S. L. Microbiome, trimethylamine N-oxide, and cardiometabolic disease. *Transl. Res. J. Lab. Clin. Med.* **179**, 108–115 (2017).
4. Dinicolantonio, J. J., McCarty, M. & Okeefe, J. Association of moderately elevated trimethylamine N-oxide with cardiovascular risk: Is TMAO serving as a marker for hepatic insulin resistance. *Open Heart* **6**, e000890–e000890 (2019).
5. Hoyles, L. *et al.* Metabolic retroconversion of trimethylamine N-oxide and the gut microbiota. *Microbiome* **6**, 73–73 (2018).
6. Zeisel, S. H., Wishnok, J. S. & Blusztajn, J. K. Formation of methylamines from ingested choline and lecithin. *J. Pharmacol. Exp. Ther.* **225**, 320–324 (1983).
7. Kühn, T. *et al.* Intra-individual variation of plasma trimethylamine-N-oxide (TMAO), betaine and choline over 1 year. *Clin. Chem. Lab. Med. CCLM* **55**, 261–268 (2017).
8. Duranton, F. *et al.* Normal and pathologic concentrations of uremic toxins. *J. Am. Soc. Nephrol. JASN* **23**, 1258–70 (2012).
9. Bain, M., Faull, R., Fornasini, G., Milne, R. & Evans, A. Accumulation of Trimethylamine and trimethylamine-N-oxide in End-Stage Renal Disease Patients Undergoing Haemodialysis. *Nephrol. Dial. Transplant. Off. Publ. Eur. Dial. Transpl. Assoc. - Eur. Ren. Assoc.* **21**, 1300–4 (2006).
10. Tang, W. H. W. *et al.* Intestinal microbial metabolism of phosphatidylcholine and cardiovascular risk. *N. Engl. J. Med.* **368**, 1575–1584 (2013).
11. Tang, W. H. W. *et al.* Prognostic value of elevated levels of intestinal microbe-generated metabolite trimethylamine-N-oxide in patients with heart failure: refining the gut hypothesis. *J. Am. Coll. Cardiol.* **64**, 1908–1914 (2014).
12. Wang, Z. *et al.* Non-lethal Inhibition of Gut Microbial Trimethylamine Production for the Treatment of Atherosclerosis. *Cell* **163**, 1585–1595 (2015).
13. Zhu, W. *et al.* Gut Microbial Metabolite TMAO Enhances Platelet Hyperreactivity and Thrombosis Risk. *Cell* **165**, 111–124 (2016).
14. Aldana-Hernández, P. *et al.* Dietary Choline or Trimethylamine N-oxide Supplementation Does Not Influence Atherosclerosis Development in Ldlr−/− and Apoe−/− Male Mice. *J. Nutr.* (2019) doi:10.1093/jn/nxz214.

15. Miller, C. A. *et al.* Effect of egg ingestion on trimethylamine-N-oxide production in humans: a randomized, controlled, dose-response study. *Am. J. Clin. Nutr.* **100**, 778–786 (2014).
16. Jia, J. *et al.* Assessment of Causal Direction Between Gut Microbiota-Dependent Metabolites and Cardiometabolic Health: Abi-Directional Mendelian Randomisation Analysis. *Diabetes* (2019) doi:10.2337/db19-0153.
17. Winther, S. A. *et al.* Utility of Plasma Concentration of Trimethylamine N-Oxide in Predicting Cardiovascular and Renal Complications in Individuals With Type 1 Diabetes. *Diabetes Care* **42**, 1512–1520 (2019).
18. Huc, T. *et al.* Chronic, low-dose TMAO treatment reduces diastolic dysfunction and heart fibrosis in hypertensive rats. *Am. J. Physiol.-Heart Circ. Physiol.* **315**, H1805–H1820 (2018).
19. Collins, H. L. *et al.* L-Carnitine intake and high trimethylamine N-oxide plasma levels correlate with low aortic lesions in ApoE−/− transgenic mice expressing CETP. *Atherosclerosis* **244**, 29–37 (2016).
20. Zhao, Z.-H. *et al.* Trimethylamine N-oxide attenuates high-fat high-cholesterol diet-induced steatohepatitis by reducing hepatic cholesterol overload in rats. *World J. Gastroenterol.* **25**, 2450–2462 (2019).
21. Dumas, M.-E. *et al.* Microbial-Host Co-metabolites Are Prodromal Markers Predicting Phenotypic Heterogeneity in Behavior, Obesity, and Impaired Glucose Tolerance. *Cell Rep.* **20**, 136–148 (2017).
22. Jaworska, K., Bielinska, K., Gawrys-Kopczynska, M. & Ufnal, M. TMA (trimethylamine), but not its oxide TMAO (trimethylamine-oxide), exerts haemodynamic effects: implications for interpretation of cardiovascular actions of gut microbiome. *Cardiovasc. Res.* **115**, 1948–1949 (2019).
23. Huo, X. *et al.* Trimethylamine N-Oxide Metabolites in Early Pregnancy and Risk of Gestational Diabetes: A Nested Case-Control Study. *J. Clin. Endocrinol. Metab.* **104**, 5529–5539 (2019).
24. Poly, C. *et al.* The relation of dietary choline to cognitive performance and white-matter hyperintensity in the Framingham Offspring Cohort. *Am. J. Clin. Nutr.* **94**, 1584–1591 (2011).
25. Nurk, E. *et al.* Plasma free choline, betaine and cognitive performance: the Hordaland Health Study. *Br. J. Nutr.* **109**, 511–519 (2013).

735 26. Leathwood, P. D., Heck, E. & Mauron, J. Phosphatidyl choline and avoidance
736 performance in 17 month-old SEC/1ReJ mice. *Life Sci.* **30**, 1065–1071 (1982).
737 27. Bartus, R. T., Dean, R. L., Goas, J. A. & Lippa, A. S. Age-related changes in passive
738 avoidance retention: modulation with dietary choline. *Science* **209**, 301–3 (1980).
739 28. Vogt, N. M. *et al.* The gut microbiota-derived metabolite trimethylamine N-oxide is
740 elevated in Alzheimer's disease. *Alzheimers Res. Ther.* **10**, 124–124 (2018).
741 29. Gao, Q. *et al.* Decreased levels of circulating trimethylamine N-oxide alleviate
742 cognitive and pathological deterioration in transgenic mice: A potential therapeutic
743 approach for Alzheimer's disease. *Aging* **11**, 8642–8663 (2019).
744 30. Weksler, B. B. *et al.* Blood-brain barrier-specific properties of a human adult brain
745 endothelial cell line. *FASEB J. Off. Publ. Fed. Am. Soc. Exp. Biol.* **19**, 1872–4
746 (2005).
747 31. Maggioli, E. *et al.* Estrogen protects the blood-brain barrier from inflammation-
748 induced disruption and increased lymphocyte trafficking. *Brain. Behav. Immun.* **51**,
749 212–222 (2015).
750 32. Abbott, N. J., Hughes, C. C., Revest, P. A. & Greenwood, J. Development and
751 characterisation of a rat brain capillary endothelial culture: towards an in vitro
752 blood-brain barrier. *J. Cell Sci.* **103 (Pt 1**, 23–37 (1992).
753 33. Coisne, C. *et al.* Mouse syngenic in vitro blood-brain barrier model: a new tool to
754 examine inflammatory events in cerebral endothelium. *Lab. Investig. J. Tech.*
755 *Methods Pathol.* **85**, 734–46 (2005).
756 34. Pais de Barros, J.-P. *et al.* Quantitative lipopolysaccharide analysis using
757 HPLC/MS/MS and its combination with the limulus amebocyte lysate assay. *J.*
758 *Lipid Res.* **56**, 1363–9 (2015).
759 35. Gautier, L., Cope, L., Bolstad, B. M. & Irizarry, R. A. affy--analysis of Affymetrix
760 GeneChip data at the probe level. *Bioinforma. Oxf. Engl.* **20**, 307–15 (2004).
761 36. Chen, E. Y. *et al.* Enrichr: interactive and collaborative HTML5 gene list enrichment
762 analysis tool. *BMC Bioinformatics* **14**, 128–128 (2013).
763 37. Kuleshov, M. V. *et al.* Enrichr: a comprehensive gene set enrichment analysis web
764 server 2016 update. *Nucleic Acids Res.* **44**, W90-7 (2016).
765 38. Tarca, A. L. *et al.* A novel signaling pathway impact analysis. *Bioinforma. Oxf. Engl.*
766 **25**, 75–82 (2009).
767 39. Hoyles, L. *et al.* Molecular phenomics and metagenomics of hepatic steatosis in
768 non-diabetic obese women. *Nat. Med.* **24**, 1070–1080 (2018).

40. Zhang, J. D. & Wiemann, S. KEGGgraph: a graph approach to KEGG PATHWAY in R and bioconductor. *Bioinforma. Oxf. Engl.* **25**, 1470–1471 (2009).
41. McArthur, S. *et al.* Annexin A1: a central player in the anti-inflammatory and neuroprotective role of microglia. *J Immunol* **185**, 6317–6328 (2010).
42. Wishart, D. S. *et al.* HMDB 4.0: the human metabolome database for 2018. *Nucleic Acids Res.* **46**, D608–D617 (2018).
43. Marottoli, F. M. *et al.* Peripheral Inflammation, Apolipoprotein E4, and Amyloid-β Interact to Induce Cognitive and Cerebrovascular Dysfunction: *ASN Neuro* (2017) doi:10.1177/1759091417719201.
44. Kim, D., Langmead, B. & Salzberg, S. L. HISAT: a fast spliced aligner with low memory requirements. *Nat. Methods* **12**, 357–360 (2015).
45. Liao, Y., Smyth, G. K. & Shi, W. featureCounts: an efficient general purpose program for assigning sequence reads to genomic features. *Bioinforma. Oxf. Engl.* **30**, 923–930 (2014).
46. Hölter, S. M. *et al.* Tests for Anxiety-Related Behavior in Mice. *Curr. Protoc. Mouse Biol.* **5**, 291–309 (2015).
47. Davis, K. E., Eacott, M. J., Easton, A. & Gigg, J. Episodic-like memory is sensitive to both Alzheimer's-like pathological accumulation and normal ageing processes in mice. *Behav. Brain Res.* **254**, 73–82 (2013).
48. Leger, M. *et al.* Object recognition test in mice. *Nat. Protoc.* **8**, 2531–2537 (2013).
49. Denninger, J. K., Smith, B. M. & Kirby, E. D. Novel Object Recognition and Object Location Behavioral Testing in Mice on a Budget. *J. Vis. Exp. JoVE* (2018) doi:10.3791/58593.
50. Thomas, R., Morris, A. W. J. & Tai, L. M. Epidermal growth factor prevents APOE4-induced cognitive and cerebrovascular deficits in female mice. *Heliyon* **3**, e00319 (2017).
51. Love, M. I., Huber, W. & Anders, S. Moderated estimation of fold change and dispersion for RNA-seq data with DESeq2. *Genome Biol.* **15**, 550 (2014).
52. Lochhead, J. J., Yang, J., Ronaldson, P. T. & Davis, T. P. Structure, Function, and Regulation of the Blood-Brain Barrier Tight Junction in Central Nervous System Disorders. *Front. Physiol.* **11**, 914 (2020).
53. Cristante, E. *et al.* Identification of an essential endogenous regulator of blood-brain barrier integrity, and its pathological and therapeutic implications. *Proc. Natl. Acad. Sci. U. S. A.* **110**, 832–841 (2013).

803 54. McArthur, S. *et al.* Annexin A1 regulates hormone exocytosis through a mechanism
804 involving actin reorganization. *FASEB J* **23**, 4000–4010 (2009).
805 55. Bena, S., Brancaleone, V., Wang, J. M., Perretti, M. & Flower, R. J. Annexin A1
806 interaction with the FPR2/ALX receptor: identification of distinct domains and
807 downstream associated signaling. *J. Biol. Chem.* **287**, 24690–7 (2012).
808 56. Cho, C. E. *et al.* Trimethylamine-N-oxide (TMAO) response to animal source foods
809 varies among healthy young men and is influenced by their gut microbiota
810 composition: A randomized controlled trial. *Mol. Nutr. Food Res.* **61**, 1600324
811 (2017).
812 57. Montagne, A. *et al.* Blood-Brain Barrier Breakdown in the Aging Human
813 Hippocampus. *Neuron* **85**, 296–302 (2015).
814 58. Taheri, S. *et al.* Blood-brain barrier permeability abnormalities in vascular cognitive
815 impairment. *Stroke J. Cereb. Circ.* **42**, 2158–63 (2011).
816 59. Bowman, G. L. *et al.* Blood-brain barrier impairment in Alzheimer disease: stability
817 and functional significance. *Neurology* **68**, 1809–14 (2007).
818 60. Merino, J. G. *et al.* Blood-brain barrier disruption after cardiac surgery. *AJNR Am.*
819 *J. Neuroradiol.* **34**, 518–523 (2013).
820 61. Hu, N. *et al.* Involvement of the blood-brain barrier opening in cognitive decline in
821 aged rats following orthopedic surgery and high concentration of sevoflurane
822 inhalation. *Brain Res.* **1551**, 13–24 (2014).
823 62. Abrahamov, D. *et al.* Blood-Brain Barrier Disruption After Cardiopulmonary
824 Bypass: Diagnosis and Correlation to Cognition. *Ann. Thorac. Surg.* **104**, 161–169
825 (2017).
826 63. Yang, S. *et al.* Anesthesia and Surgery Impair Blood-Brain Barrier and Cognitive
827 Function in Mice. *Front. Immunol.* **8**, 902–902 (2017).
828 64. Zenaro, E., Piacentino, G. & Constantin, G. The blood-brain barrier in Alzheimer's
829 disease. *Neurobiol. Dis.* (2016) doi:10.1016/j.nbd.2016.07.007.
830 65. Brunt, V. E. *et al.* The gut microbiome–derived metabolite trimethylamine N-oxide
831 modulates neuroinflammation and cognitive function with aging. *GeroScience*
832 (2020) doi:10.1007/s11357-020-00257-2.
833 66. He, W. *et al.* Trimethylamine N-Oxide, a Gut Microbiota-Dependent Metabolite, is
834 Associated with Frailty in Older Adults with Cardiovascular Disease. *Clin. Interv.*
835 *Aging* **15**, 1809–1820 (2020).

836 67. Zhu, C. *et al.* Association of plasma trimethylamine-N-oxide levels with post-stroke
837 cognitive impairment: a 1-year longitudinal study. *Neurol. Sci. Off. J. Ital. Neurol.*
838 *Soc. Ital. Soc. Clin. Neurophysiol.* **41**, 57–63 (2020).
839 68. Zhao, L. *et al.* Higher Circulating Trimethylamine N-oxide Sensitizes Sevoflurane-
840 Induced Cognitive Dysfunction in Aged Rats Probably by Downregulating
841 Hippocampal Methionine Sulfoxide Reductase A. *Neurochem. Res.* **44**, 2506–
842 2516 (2019).
843 69. Meng, F., Li, N., Li, D., Song, B. & Li, L. The presence of elevated circulating
844 trimethylamine N-oxide exaggerates postoperative cognitive dysfunction in aged
845 rats. *Behav. Brain Res.* **368**, 111902–111902 (2019).
846 70. Sanguinetti, E. *et al.* Microbiome-metabolome signatures in mice genetically prone
847 to develop dementia, fed a normal or fatty diet. *Sci. Rep.* **8**, (2018).
848 71. Liu, J. *et al.* Baicalin ameliorates neuropathology in repeated cerebral ischemia-
849 reperfusion injury model mice by remodeling the gut microbiota. *Aging* **12**, 3791–
850 3806 (2020).
851 72. Wang, Q.-J. *et al.* Concomitant memantine and Lactobacillus plantarum treatment
852 attenuates cognitive impairments in APP/PS1 mice. *Aging* **12**, 628–649 (2020).
853 73. Sawicka, A. K., Renzi, G. & Olek, R. A. The bright and the dark sides of L-carnitine
854 supplementation: a systematic review. *J. Int. Soc. Sports Nutr.* **17**, 49 (2020).
855 74. Chung, S. J. *et al.* Gut microbiota-derived metabolite trimethylamine N-oxide as a
856 biomarker in early Parkinson's disease. *Nutr. Burbank Los Angel. Cty. Calif* **83**,
857 111090 (2020).
858 75. Zhuang, Z. *et al.* Causal relationships between gut metabolites and Alzheimer's
859 disease: a bidirectional Mendelian randomization study. *Neurobiol. Aging* (2020)
860 doi:10.1016/j.neurobiolaging.2020.10.022.
861 76. Li, D. *et al.* Trimethylamine-N-oxide promotes brain aging and cognitive impairment
862 in mice. *Aging Cell* **17**, (2018).
863 77. Papandreou, C., Moré, M. & Bellamine, A. Trimethylamine N-Oxide in Relation to
864 Cardiometabolic Health-Cause or Effect? *Nutrients* **12**, (2020).
865 78. Zeisel, S. H. Dietary choline: biochemistry, physiology, and pharmacology. *Annu.*
866 *Rev. Nutr.* **1**, 95–121 (1981).
867 79. Lundstrom, R. C. & Racicot, L. D. Gas chromatographic determination of
868 dimethylamine and trimethylamine in seafoods. *J. - Assoc. Off. Anal. Chem.* **66**,
869 1158–1163 (1983).

80. Zeng, L.-F. *et al.* An exploration of the role of a fish-oriented diet in cognitive decline: a systematic review of the literature. *Oncotarget* **8**, 39877–39895 (2017).
81. Keenan, T. D. *et al.* Adherence to a Mediterranean diet and cognitive function in the Age-Related Eye Disease Studies 1 & 2. *Alzheimers Dement.* **16**, 831–842 (2020).
82. Zhao, W. *et al.* Fish Consumption and Stroke Risk: A Meta-Analysis of Prospective Cohort Studies. *J. Stroke Cerebrovasc. Dis. Off. J. Natl. Stroke Assoc.* **28**, 604–611 (2019).
83. Zhang, Y. *et al.* Intakes of fish and polyunsaturated fatty acids and mild-to-severe cognitive impairment risks: a dose-response meta-analysis of 21 cohort studies. *Am. J. Clin. Nutr.* **103**, 330–340 (2016).
84. Cooper, R. E., Tye, C., Kuntsi, J., Vassos, E. & Asherson, P. Omega-3 polyunsaturated fatty acid supplementation and cognition: A systematic review and meta-analysis. *J. Psychopharmacol. Oxf. Engl.* **29**, 753–763 (2015).
85. Abdelhamid, A. S. *et al.* Omega-3 fatty acids for the primary and secondary prevention of cardiovascular disease. *Cochrane Database Syst. Rev.* **11**, CD003177 (2018).
86. Gobbetti, T. & Cooray, S. N. Annexin A1 and resolution of inflammation: tissue repairing properties and signalling signature. *Biol. Chem.* **397**, 981–993 (2016).
87. Wall, R., Ross, R. P., Fitzgerald, G. F. & Stanton, C. Fatty acids from fish: the anti-inflammatory potential of long-chain omega-3 fatty acids. *Nutr. Rev.* **68**, 280–289 (2010).
88. Nicholson, J. K. *et al.* Host-gut microbiota metabolic interactions. *Science* **336**, 1262–7 (2012).
89. Needham, B. D., Kaddurah-Daouk, R. & Mazmanian, S. K. Gut microbial molecules in behavioural and neurodegenerative conditions. *Nat. Rev. Neurosci.* **21**, 717–731 (2020).

898 **Table 1.** BBB-associated genes whose expression was upregulated upon exposure
899 of hCMEC/D3 cells to TMAO.
900

Gene	Entrez ID	Description	Log_2 fold change	Category	P_{FDR}
TFRC	7037	Transferrin receptor	0.23	Transporter proteins	0.054
ABCC4	10257	ATP binding cassette subfamily C member 4	0.20	Transporter proteins	0.088
ANXA1	301	Annexin A1	0.16	Cell Adhesion/Junctional proteins/Cytoskeletal factors	0.088
CDH2	1000	Cadherin 2	0.31	Cell Adhesion/Junctional proteins/Cytoskeletal factors	0.095

901
902
903

Table 2. Daily consumption of TMAO and water in mice chronically treated with TMAO and/or LPS.

Data are mean ± standard deviation.

Variable	Sham-treated mice	LPS-treated mice	*P* value
TMAO intake (mg/day/mouse)	2.79 ± 0.38	2.82 ± 0.25	0.7
TMAO intake (mg/kg/mouse)	85.0 ± 11.4	88.9 ± 7.9	0.14
Water consumption (ml/day/mouse)	5.57 ± 0.8	5.64 ± 0.5	0.48

FIGURE LEGENDS

Fig. 1. Effects of TMAO and TMA on integrity of hCMEC/D3 cell monolayers. (A) Assessment of paracellular permeability of hCMEC/D3 monolayers to a 70 kDa FITC-dextran tracer following treatment for 24 h with varying doses of TMA (0.4 – 40 μM) or TMAO (40 – 4000 μM). Data are expressed as mean ± s.e.m., *n*=4 independent experiments. (B) Assessment of TEER of hCMEC/D3 monolayers to a 70kDa FITC-dextran tracer following treatment for 24 h with varying doses of TMA (0.4 – 40 μM) or TMAO (40 – 4000 μM). Data are expressed as mean ± s.e.m., *n*=4 independent experiments. (C) Adhesion of U937 monocytic cells to TNFα-stimulated hCMEC/D3 monolayers (10 ng/ml, 16 h) that had been treated or not for 24 h with 0.4 μM TMA or 40 μM TMAO. Data are expressed as mean ± s.e.m., *n*=3 independent experiments.

Fig. 2. Effects of TMA and TMAO on gene expression in hCMEC/D3 cells. (A) Heatmap showing expression of the 49 genes found to be significantly (P_{FDR}<0.1) differentially expressed upon exposure of hCMEC/D3 cells to 0.4 μM TMA (*n*=5 per group). (B) Heatmap showing expression of the 440 genes found to be significantly (P_{FDR}<0.1) differentially expressed upon exposure of hCMEC/D3 cells to 40 μM TMAO (*n*=5 per group). (C) Biological processes associated with genes found to be significantly upregulated (*n*=39) or downregulated (*n*=10) upon exposure of cells to TMA. (D) Biological processes of genes found to be significantly upregulated (*n*=341) or downregulated (*n*=99) upon exposure of cells to TMAO. Images in (C, D) shown based on Enrichr *P* value ranking from GO analysis. (E) Topological analysis of the KEGG networks associated with the 440 genes whose expression was significantly affected upon exposure of cells to TMAO (blue, significantly downregulated; red, significantly upregulated); genes of similar cellullar role are highlighted. (F) Confocal microscopic analysis of expression of fibrillar actin (F-actin) and the tight junction component zonula occludens-1 (ZO-1) in hCMEC/D3 cells following treatment for 24 h with 0.4 μM TMA or 40 μM TMAO. Images are representative of at least three independent experiments.

Fig. 3. Annexin A1 (ANXA1) signalling mediates effects of TMAO on hCMEC/D3 cells. (A) Total cellular expression of ANXA1 in hCMEC/D3 cells treated for 24 h with 0.4 μM TMA or 40 μM TMAO. Data are expressed as mean ± s.e.m., *n*=5-7 independent

946 experiments. (B) Medium ANXA1 content of hCMEC/D3 monolayers treated for 24 h
947 with 0.4 μM TMA or 40 μM TMAO. Data are expressed as mean ± s.e.m., *n*=3
948 independent experiments. (C) Assessment of paracellular permeability of monolayers
949 of wild-type hCMEC/D3 cells, or hCMEC/D3 cells stably transfected with either a
950 scramble shRNA sequence or an shRNA sequence targeting ANXA1 to a 70kDa FITC-
951 dextran tracer following treatment for 24 h with 40 μM TMAO. Data are expressed as
952 mean ± s.e.m., *n*=4 independent experiments. (D) Assessment of TEER of
953 monolayers of wild-type hCMEC/D3 cells, or hCMEC/D3 cells stably transfected with
954 either a scramble shRNA sequence or an shRNA sequence targeting ANXA1 following
955 treatment for 24 h with 40 μM TMAO. Data are expressed as mean ± s.e.m., *n*=4
956 independent experiments. (E) Assessment of paracellular permeability of hCMEC/D3
957 cells to a 70kDa FITC-dextran tracer following treatment for 24 h with 40 μM TMAO,
958 with or without 10 min pre-treatment with the FPR2 antagonist WRW_4 (10 μM). Data
959 are expressed as mean ± s.e.m., *n*=3 independent experiments. (F) Assessment of
960 TEER of hCMEC/D3 cells following treatment for 24 h with 40 μM TMAO, with or
961 without 10 min pre-treatment with the FPR2 antagonist WRW4 (10 μM). Data are
962 expressed as mean ± s.e.m., *n*=3 independent experiments.
963
964 **Fig. 4.** Acute treatment with TMAO promotes BBB integrity *in vivo*. (A) Extravasation
965 of Evans blue dye into brain parenchyma over a 1 h period in 2-month-old male
966 C57Bl/6J mice following i.p. injection of 1.8 mg/kg TMAO for 2 h, 6 h or 24 h *vs.* a
967 saline injected control. Data are normalised to plasma Evans blue content, and are
968 expressed as mean ± s.e.m., *n*=5-6 mice. (B) Extravasation of Evans blue dye into
969 brain parenchyma over a 1 h period in 2-month-old male C57Bl/6J mice following i.p.
970 injection of saline or E. coli O111:B4 LPS (3 mg/kg) with or without subsequent i.p.
971 injection of 1.8 mg/kg TMAO according to the schedule shown. Data are normalised
972 to plasma Evans blue content, and are expressed as mean ± s.e.m., *n*=4-6 mice.
973
974 **Fig. 5.** Acute exposure of mice to TMAO significantly alters the whole brain
975 transcriptome. (A) Heatmap showing expression of the 76 genes found to be
976 significantly (P_{FDR}<0.1) differentially expressed in the mouse brain after 2 h exposure
977 to 1.8 mg/kg TMAO (*n*=3 per group). Data were scaled by row. (B) Over-representation
978 analysis (Enrichr) showing KEGG pathways associated with the 76 genes. (C)

Comparative analysis of significantly differentially expressed genes identified groupings associated with distinct biological functions. (D) Among the 197 BBB-specific genes identified in the data set, only *App* and *Cpe* were significantly (P_{FDR}<0.1) differentially expressed in the mouse brain after 2 h exposure to TMAO. Data are shown as mean ± s.d, *n*=3 per group. Individual data points are not shown due to the negligible values of the s.d.

Fig. 6. Effect of long-term TMAO exposure on BBB integrity and cognitive function of mice. (A) Body weight gain in mice treated with TMAO through their drinking water (0.5 mg/ml) over 2 months, combined with a chronic low dose administration of LPS (0.5 mg/kg/week, i.p.). Data are expressed as mean ± s.e.m., *n*=8 mice, columns with different letters are significantly different at *P*<0.05. (B) Cerebellar permeability index to sodium fluorescein 2h following administration in animals previously treated with TMAO through their drinking water (0.5 mg/ml) over 2 months, combined with a chronic low dose administration of LPS (0.5 mg/kg/week, i.p.). Data are expressed as mean ± s.e.m., *n*=8 mice, columns with different letters are significantly different at *P*<0.05. (C) Typical confocal microscopic images of perivascular IgG deposition in male C57Bl/6J mice treated with TMAO through their drinking water (0.5 mg/ml) over 2 months, combined with a chronic low dose administration of LPS (0.5 mg/kg/week, i.p.). *Griffonia simplicifolia* isolectin B_4 (red) defines endothelial cells, areas of IgG deposition (white) are highlighted by arrow heads. (D) Distance travelled, (E) movement speed and (F) percentage of time in the centre as measured in the OFT in animals previously treated with TMAO through their drinking water (0.5 mg/ml) over 2 months, combined with a chronic low dose administration of LPS (0.5 mg/kg/week, i.p.). Data are expressed as mean ± s.e.m., *n*=8 mice. (G) Novel object discrimination index, calculated as described in Methods, of animals previously treated with TMAO through their drinking water (0.5 mg/ml) over 2 months, combined with a chronic low dose administration of LPS (0.5 mg/kg/week, i.p.). Data are expressed as mean ± s.e.m., *n*=8 mice, columns with different letters are significantly different at *P*<0.05. (H) Percentage of spontaneous alternation and (I) total distance travelled in the Y-maze test for animals previously treated with TMAO through their drinking water (0.5 mg/ml) over 2 months, combined with a chronic low dose administration of LPS (0.5 mg/kg/week, i.p.). Data are expressed as mean ± s.e.m., *n*=8 mice.

Supplementary Fig. 1. Confirmation of ANXA1 targeting and knock-down in hCMEC/D3 cells stably transfected with appropriate shRNA sequences. (A) Typical flow cytometric profiles of wild-type cells, cells transfected with a scramble shRNA sequence and cells transfected with an ANXA1-targeting shRNA sequence, alongside unstained and second antibody controls. (B) Expression of ANXA1 in wild-type hCMEC/D3 cells, cells transfected with a scramble shRNA sequence and cells transfected with an ANXA1-targeting shRNA sequence. Data are expressed as mean ± s.e.m., *n*=4 independent experiments.

Supplementary Fig. 2. Neither TMAO nor TMA treatment affected the major endothelial efflux transporters BCRP or P-glycoprotein. (A-D) *In vitro* analysis revealed no significant effects of either TMAO or TMA upon BCRP (A, C) or P-glycoprotein (B, D) activity. Dashed lines represent Loess regression fits, with shading representing 95% confidence intervals. (E) hCMEC/D3 cell surface expression of BCRP was unaffected by 24 h exposure to TMA (0.4 μM) or TMAO (40 μM). Data are expressed as mean ± s.e.m., *n*=3 independent experiments. (F) hCMEC/D3 cell surface expression of P-glycoprotein was unaffected by 24 h exposure to TMA (0.4 μM) or TMAO (40 μM). Data are expressed as mean ± s.e.m., *n*=3 independent experiments.

Supplementary Fig. 3. *In vitro* (hCMEC/D3 cell) *FMO3* gene expression is unaffected by exposure to TMA (0.4 μM) or TMAO (40 μM). Dark blue lines represent the standard deviation (+/-). There was no statistically significant difference between TMA and the control, nor between TMAO and the control (Supplementary Tables 2 and 3). Individual data points are not shown due to the negligible values of the standard deviations.

Supplementary Fig. 4. Neither chronic low-dose LPS nor TMAO treatment significantly increases serum inflammatory cytokines. (A) Serum TNFα concentrations in male C57Bl/6J mice treated with TMAO through their drinking water (0.5 mg/ml) over 2 months, combined with a chronic low dose administration of LPS (0.5 mg/kg/week, i.p.). Data are expressed as mean ± s.e.m., *n*=7-8 mice. (B) Serum IL-1β concentrations in male C57Bl/6J mice treated with TMAO through their drinking water (0.5 mg/ml) over 2 months, combined with a chronic low dose administration of

LPS (0.5 mg/kg/week, i.p.). Data are expressed as mean ± s.e.m., *n*=7-8 mice.

Supplementary Table 1. Normalized microarray data for hCMEC/D3 treated or not with TMA (0.4 µM) or TMAO (40 µM)

Supplementary Table 2. Differential gene expression for control compared with TMA treatment, as assessed using LIMMA

Supplementary Table 3. Differential gene expression for control compared with TMAO treatment, as assessed using LIMMA

Supplementary Table 4. KEGG-based SPIA of genes whose expression was significantly affected by TMAO

Supplementary Table 5. GO (biological process) analysis of TMA-up-regulated genes as assessed using Enrichr

Supplementary Table 6. GO (biological process) analysis of TMA-down-regulated genes as assessed using Enrichr

Supplementary Table 7. GO (biological process) analysis of TMAO-up-regulated genes as assessed using Enrichr

Supplementary Table 8. GO (biological process) analysis of TMAO-down-regulated genes as assessed using Enrichr

Supplementary Table 9. Differential gene expression of BBB-associated genes (*in vitro* TMA treatment)

Supplementary Table 10. Differential gene expression of BBB-associated genes (*in vitro* TMAO treatment)

Supplementary Table 11. Differential gene expression in mouse brain for control compared with TMAO treatment, as assessed using DESeq2

Supplementary Table 12. Differential expression of BBB-associated genes in mouse brain for control compared with TMAO treatment, as assessed using DESeq2

Figure 1

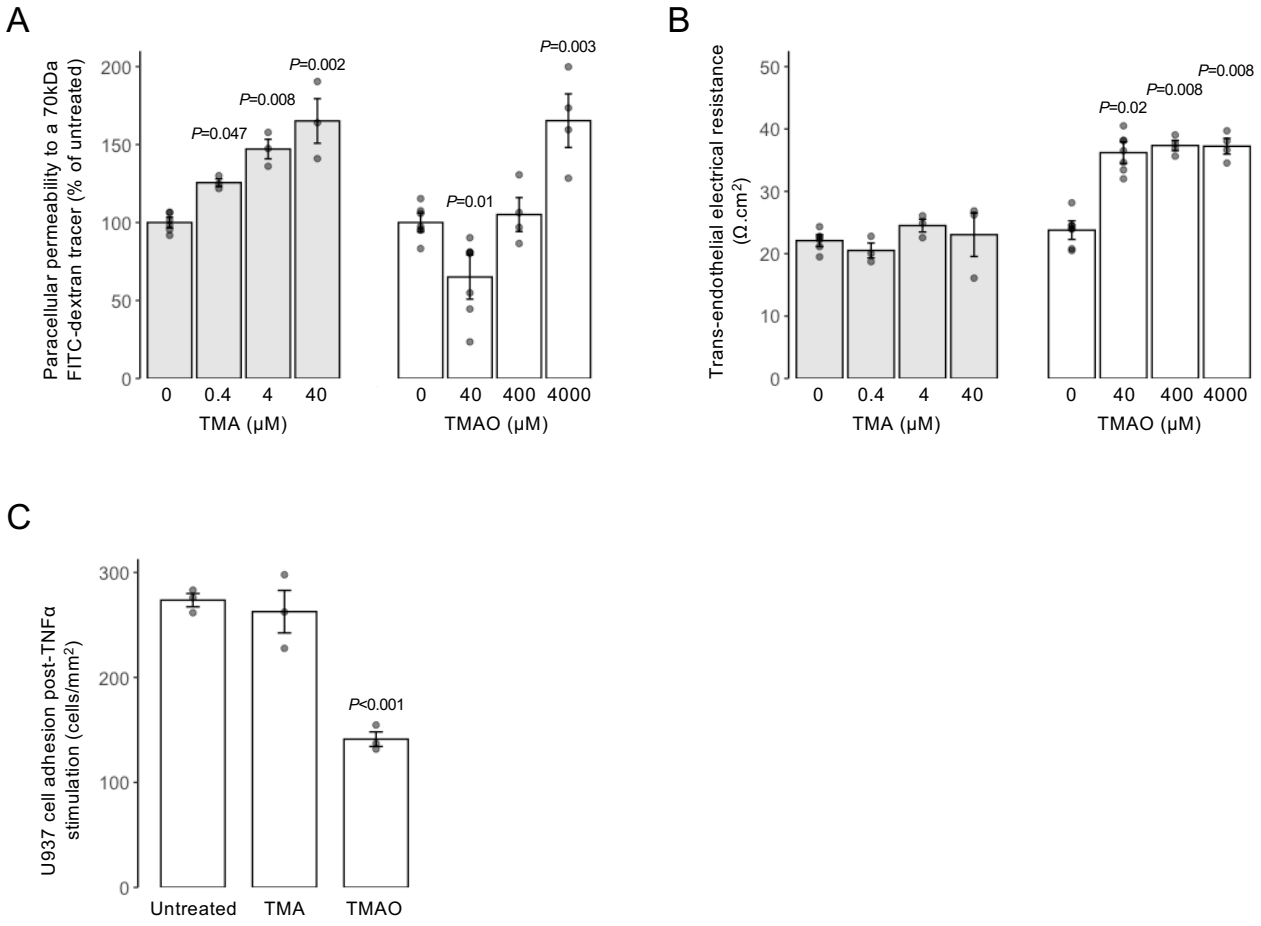

Figure 2

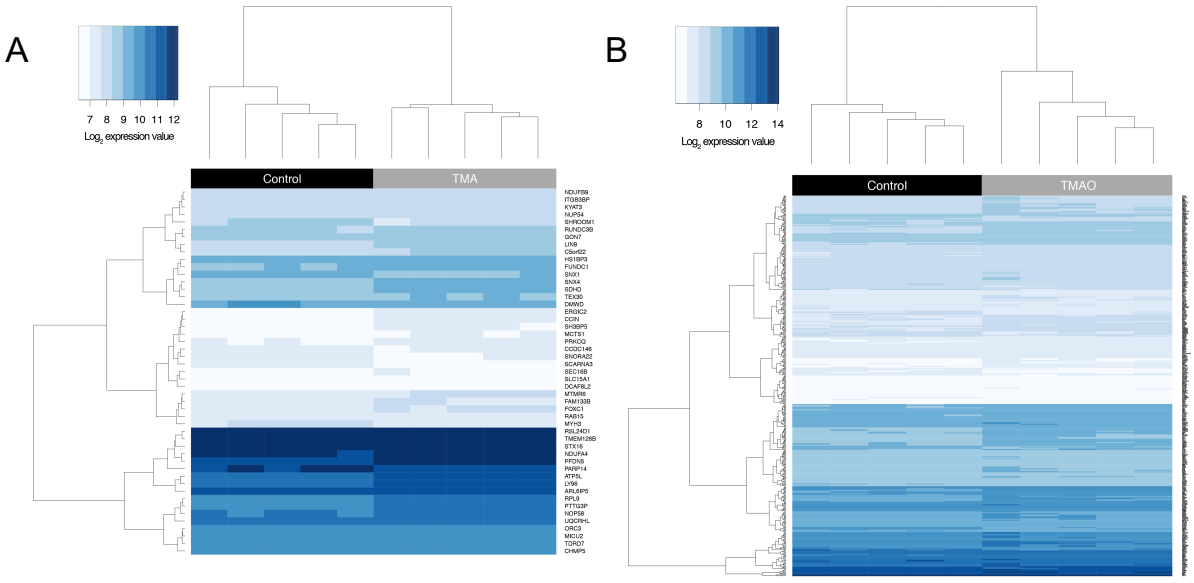

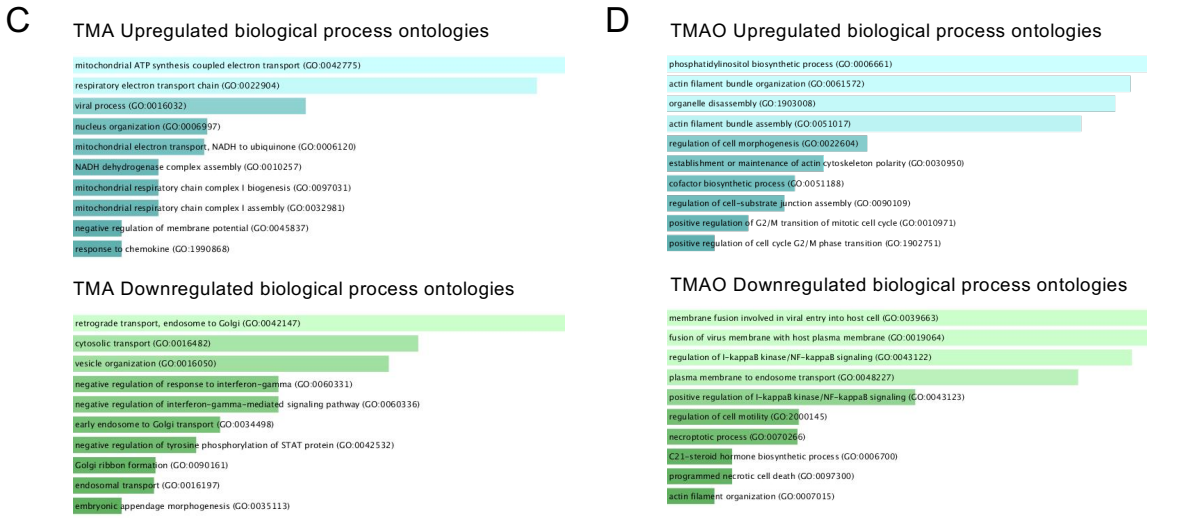

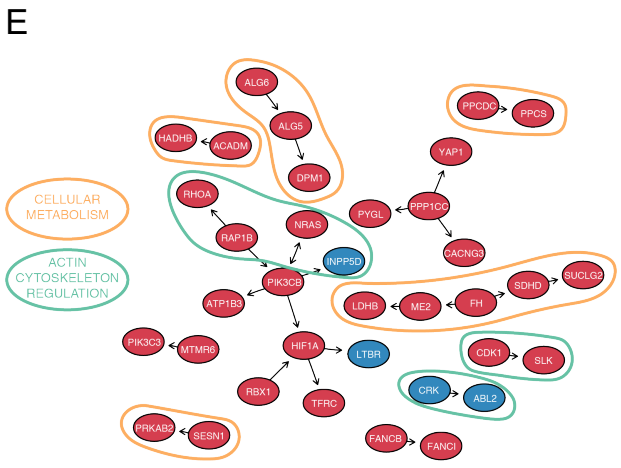

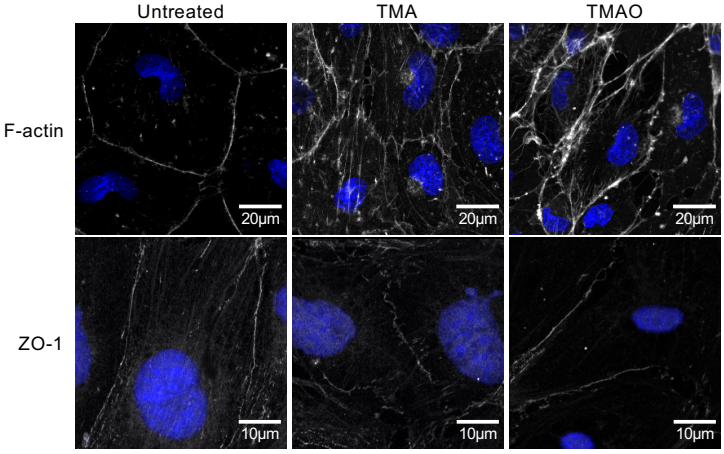

Figure 3

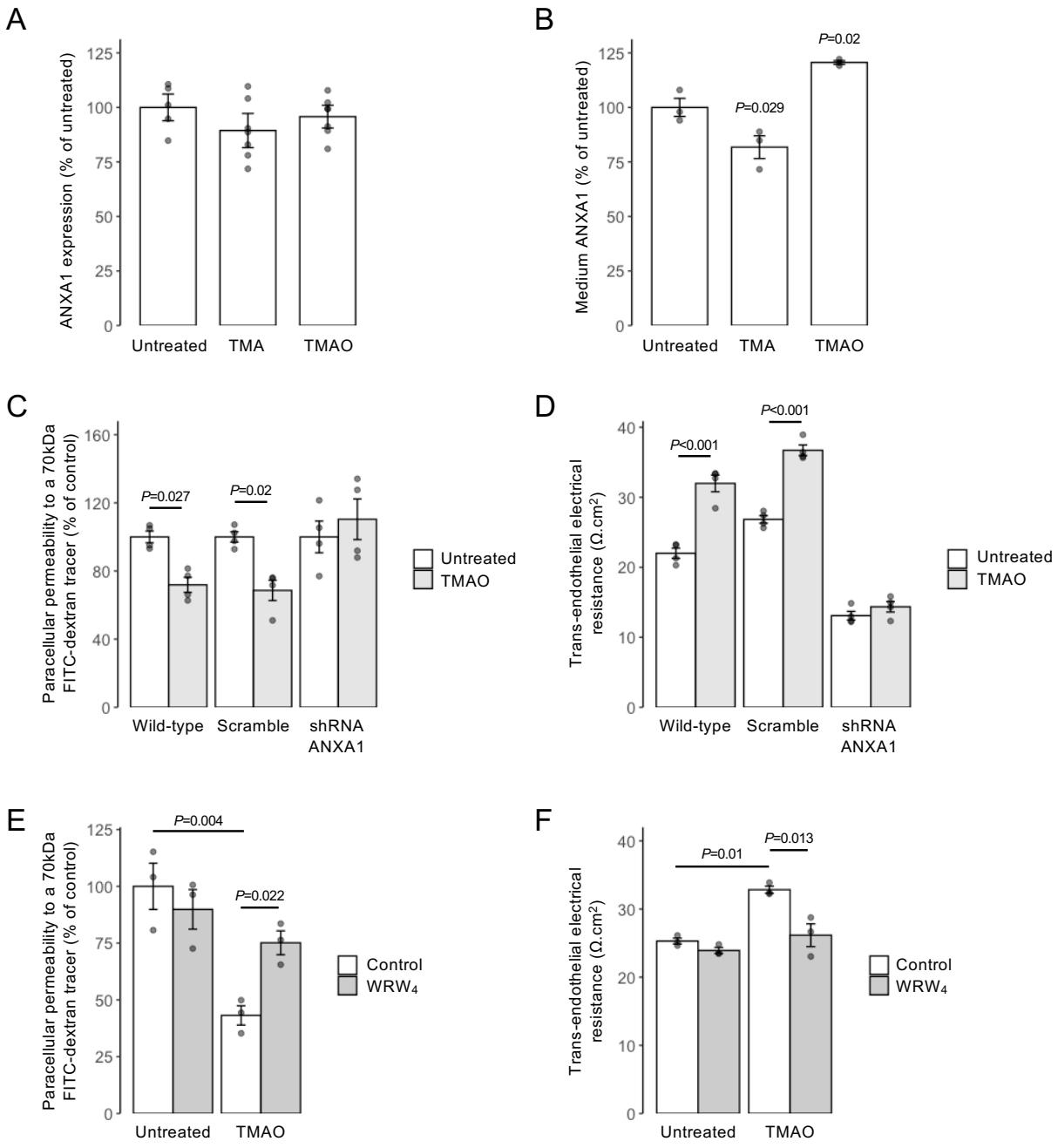

Figure 4

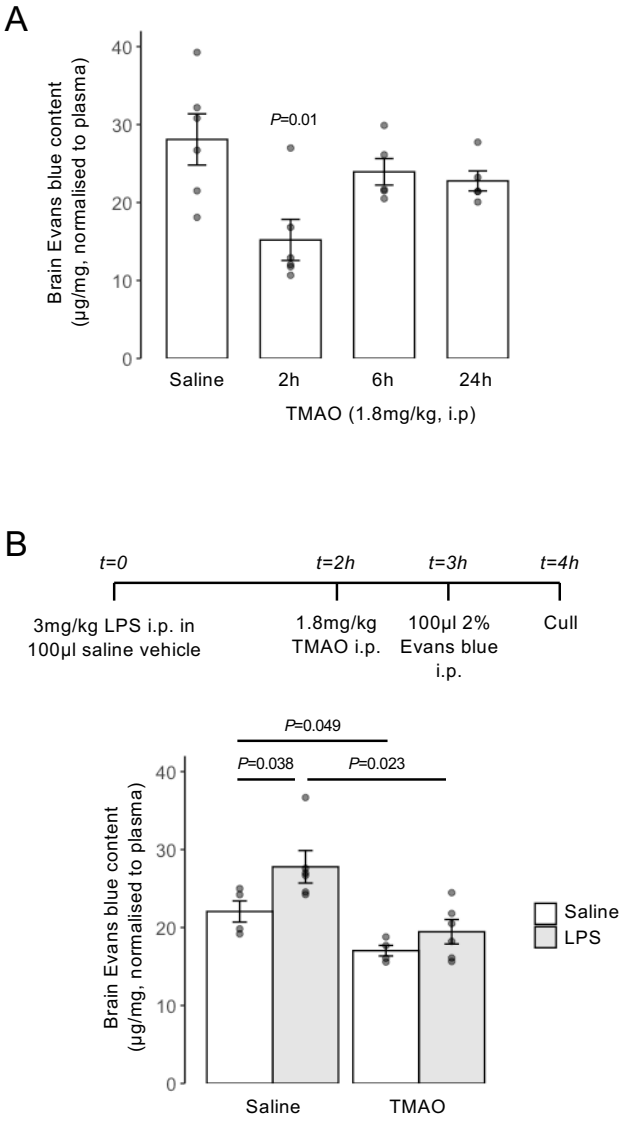

Figure 5

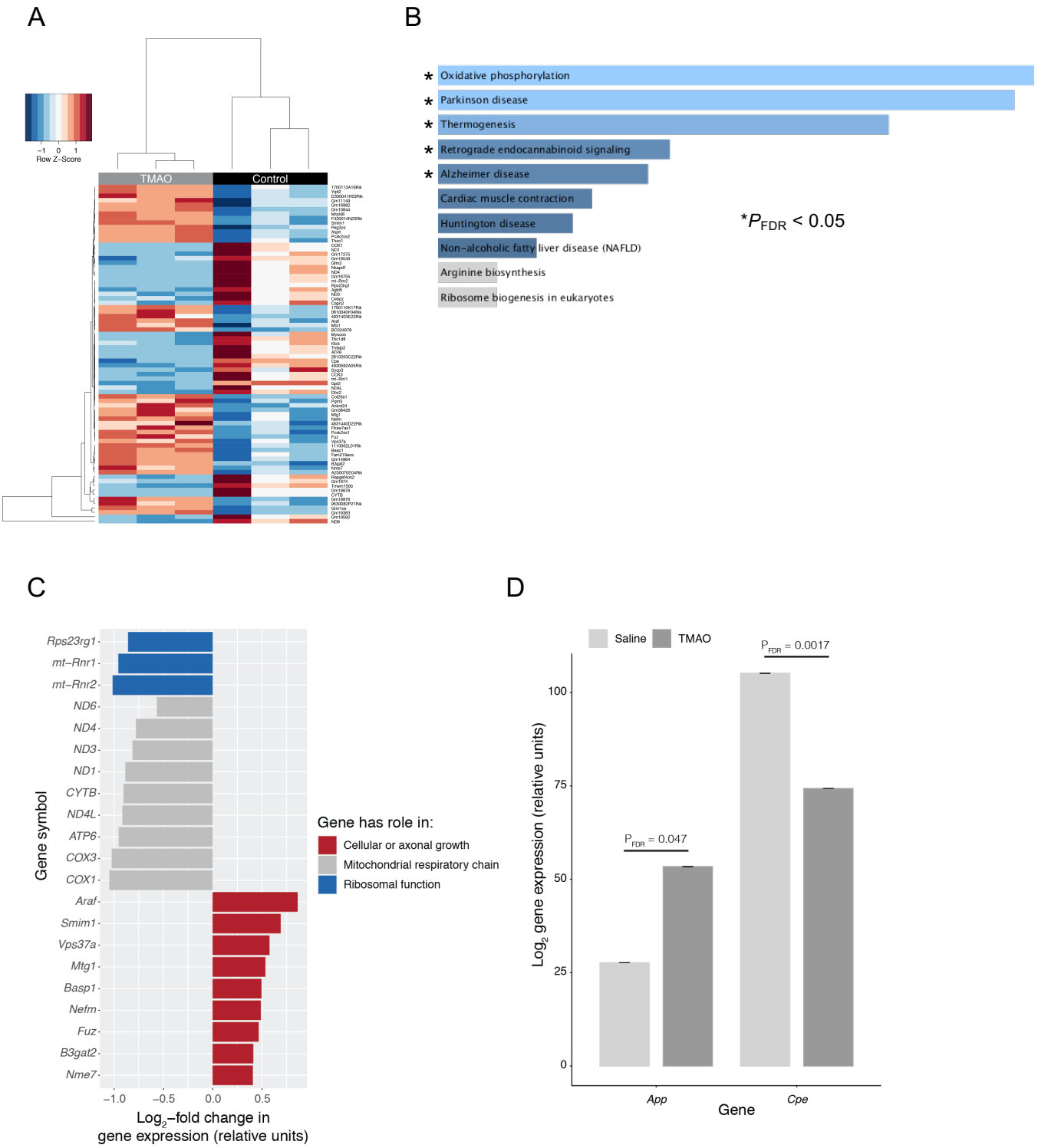

Figure 6

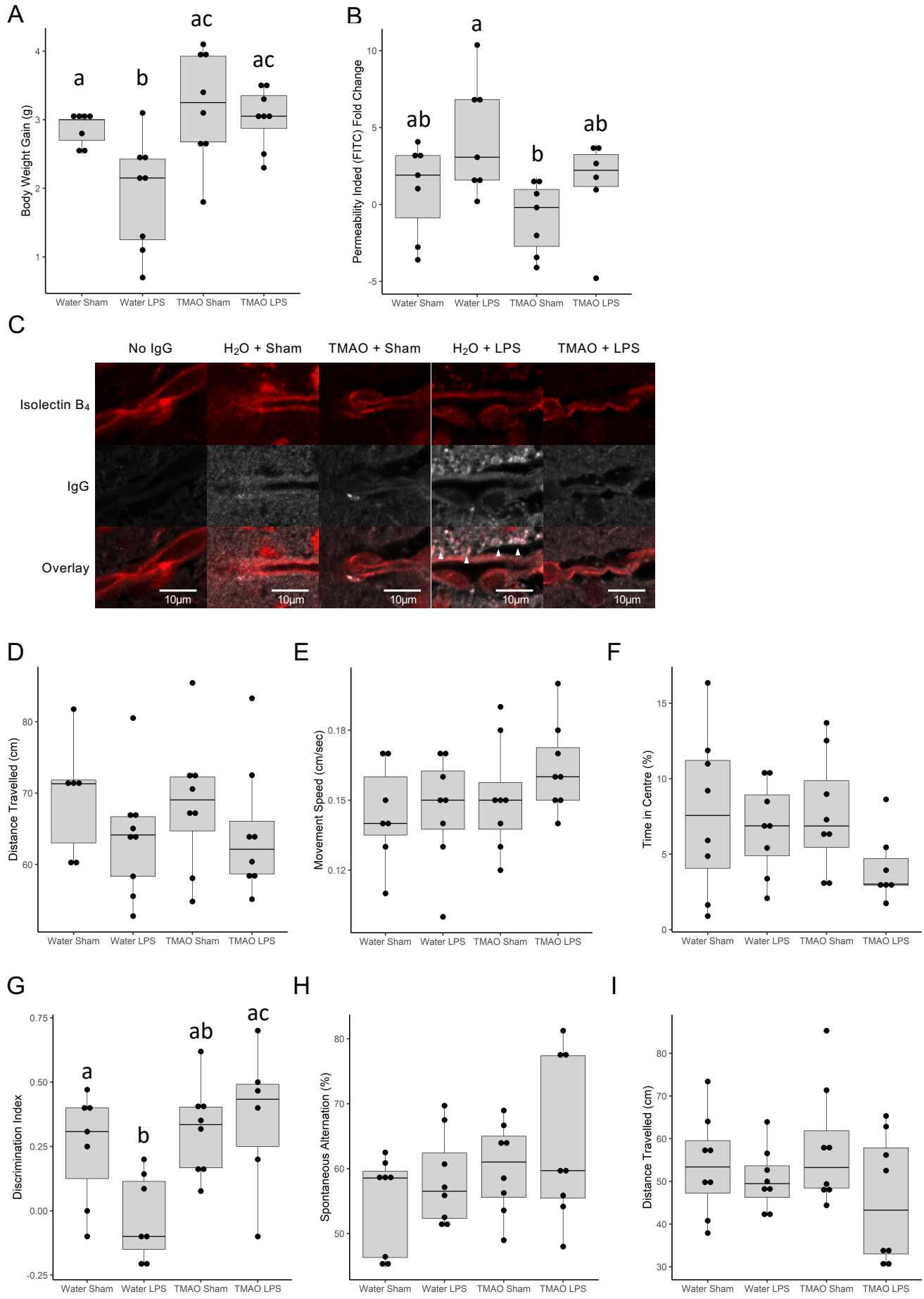

Supplementary Figure 1

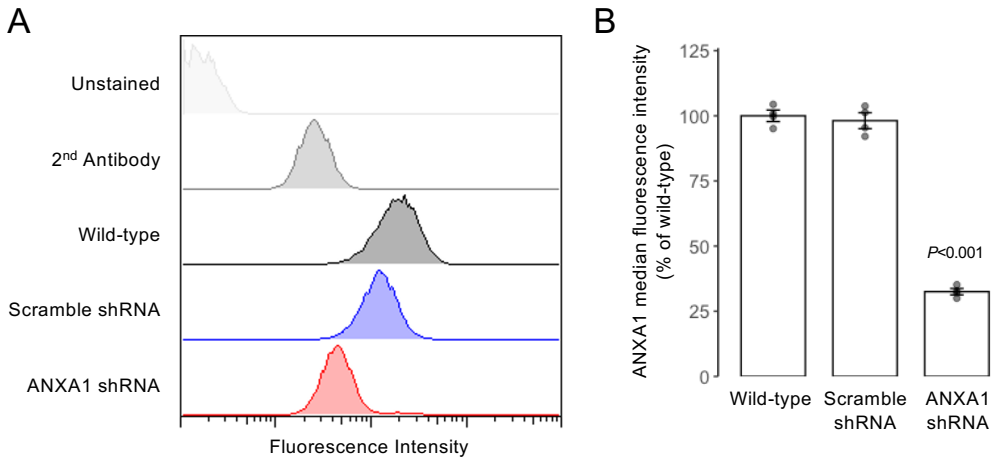

Supplementary Figure 2

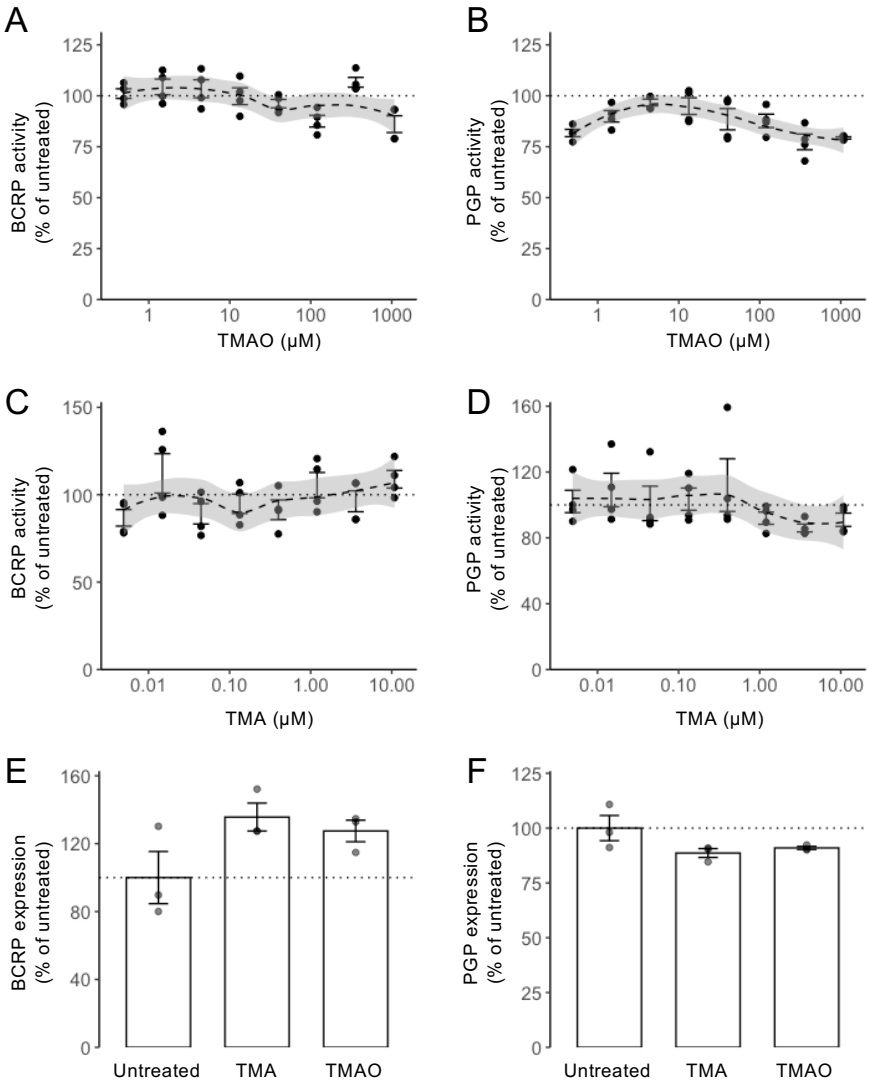

Supplementary Figure 3

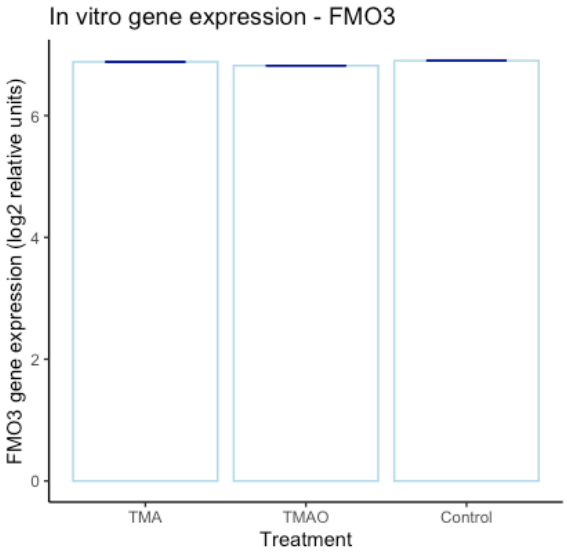

Supplementary Figure 4